THINK INDIA JOURNAL

ISSN:0971-1260

Vol-22-Issue-22-December-2019

PHASE CONGRUENCY

Patil Nitin Santosh[1] and Dr. V.Balakrishna Reddy[2]

Research Scholar[1] and Professor[2], Swami Vivekanand University, Sagar, Madhya Pradesh

ABSTRACT

This paper presents a frequency-domain analysis tool called phase congruency. An overview of what is required from phase congruency, its purpose in fusion and the goals provides a detailed formulation of phase congruency; each step is discussed in the context of multi-spectral information and the goal of extracting a stable measure to compare the disparate modalities. An investigation which aims to identify predictable quantities extracted in the phase congruency analysis process is specified and carried out. it clarifies the objectives of this investigation and the approach to achieving them. . Thermal images appear very different from the familiar visible spectrum, material boundaries and object edges still make elements in the scene recognisable to the human eye. This observation motivates the use of structural features (e.g. edges, contours and corners) as stable and matchable elements of multi-spectral scenes. Edges are commonly extracted using the Canny edge detector in which linear filtering with a heuristic threshold is used to detect edges at points of high contrast, i.e. a large gradient magnitude between adjacent pixels is used to indicate the presence of an edge. The undesired effect of this method is that areas of low contrast are left devoid of features and, due to the xed-size filter, blurred edges are poorly localized Thermal images in particular often contain large areas of low contrast, and edges are often blurred due to the low spatial resolution and thermal phenomena .Therefore, structural features cannot be repeatable detected or compared using conventional gradient-based methods.

Keywords: Congruency, Phase Angle, Phase Deviation, Angular Distance, SVM, RBF, ROC, TPR

INTRODUCTION

Phase congruency is an extension of the local energy model, which utilises the relationship between structural (or spatial) features in images and their underlying Fourier components . This earlier formulation of phase congruency found limited success due to its sensitivity to noise and poor localization of features however, a number of works have extended this theoretical base to provide a measure of absolute structural signficance particularly well suited to detecting spatial features in natural scenes with large areas of low contrast Its use in multi-spectral imaging is motivated by its independence from image contrast, ability to accurately localise features in images with low spatial resolution and robustness against image noise.

This paper presents an investigation into the phase congruency process with two objectives. The first is to develop an invariant representation which depicts the stable information shared by both spectral modalities. Creating a visually similar representation allows methods that compare visual similarity between regions to be adapted to function in any spectral range by incorporating phase congruency as a preliminary stage of processing. The second objective is the focus of the investigation and is aimed at identifying predictable relationships between elements exposed in the phase congruency analysis process. Extracting information that can be used to reliably compare the disparate modalities is an important step towards matching corresponding points captured by the distinct sensors. Phase congruency is calculated on images using directional (oriented) log-Gabor multi-scale filter banks in which each point is analysed individually within the context of its neighbours. An overview of the aims of the phase congruency process is provided inFrequency-domain analysis is performed using a series of multi-scale filter banks; introduces the adapted Gabor filters used to perform this analysis on each pixel. Phase congruency is initially formulated in one dimension and is then extended to two dimensions for use in image processing. A final stage of computation, presented condenses the directional congruency values into a reduced feature set which describes the invariant information in the visible and thermal spectra.

MULTI-SCALE CONGRUENCY ON A ONE DIMENSIONAL SIGNAL

ISSN:0971-1260

Vol-22-Issue-22-December-2019

Phase congruency assigns an absolute significance to points where the Fourier components are maximally in phase this implies that frequency components exist over a broad range of the spectrum and that there is consensus of local phase between the components. The following sections formulate the phase congruency measure.

Filter response

At each point in the signal, the log-Gabor filter bank generates a set of even and odd response vectors at each scale. Components of the response vector, $e_n(x)$ and $o_n(x)$, are formed by convolving the quadrature pairs of even and odd filters at each scale n with the underlying signal information. The filter responses are described in terms of the amplitude, A_n, and phase, $_n$, at each scale defined by

A small constant, , is included in the denominator to avoid division by 0. Frequency spread is incorporated into a weighting function which is used to penalise points where there is a narrow range of frequencies

W (x) = (1 + e (c s(x)) 1: (7)

Parameters c and control the cut-o (below which the phase congruency value is penalised) and the steepness of the curve respectively. The weighting function is plotted in Fig. 1

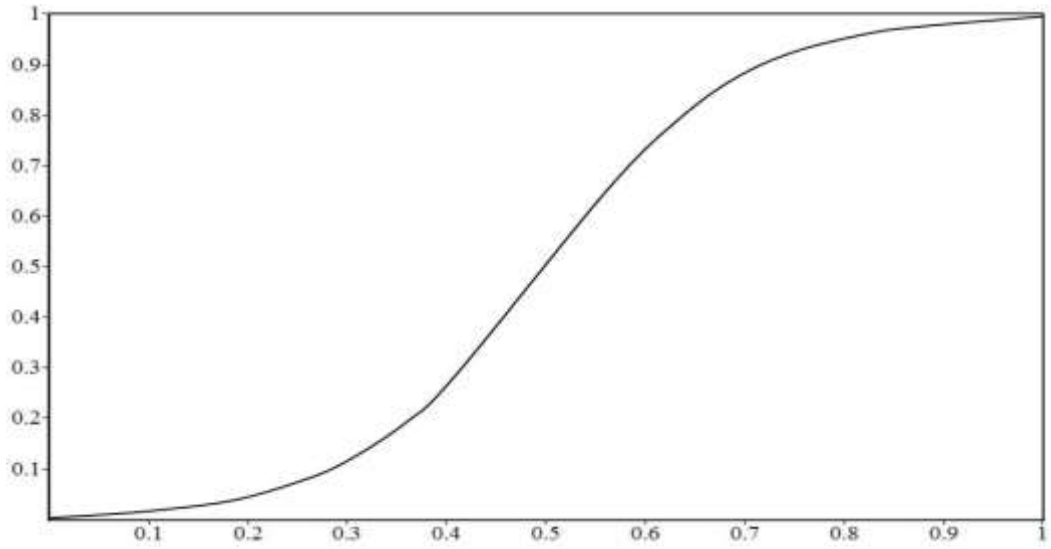

Figure-1: Multi-scale weighting function used to calculate frequency spread from filter response magnitudes Values below the cuto parameter, c, are penalised. (In this case c = :5 and = 10.)

Note that this measure is based on the relative weighting of filter responses and is independent of the intensity information (i.e. gradient magnitude or brightness) of the image.

Quantifying consensus on underlying structure

Local phase is based on the ratio of quadrature filter responses at each scale, and is often depicted, described and compared as an angular quantity (shown in Eq. (5b)). Phase is an indication of the underlying structure at a point in the signal. As congruency occurs at points where the Fourier components are maximally in phase, a means of quantifying the consensus of these components is required:

The mean phase angle is a normalized direction vector representing the combined phase consensus over multiple scales and is defined as:

$$= \frac{1}{P\ (\ _ne_n)^2 + (\ _no_n)^2)_n}\ (\ _ne_n; \qquad (8)$$

Phase consensus is quantified by calculating the average (mean) phase angle and then weighting each filter response magnitude A_n with the vector's deviation from this mean phase angle.

ISSN:0971-1260

Vol-22-Issue-22-December-2019

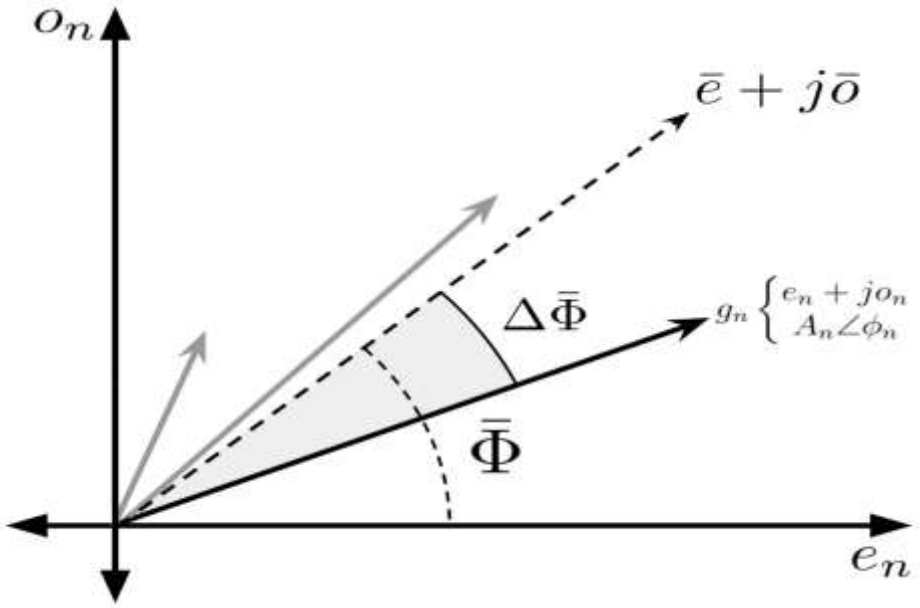

Figure-2: The mean phase angle is calculated using the filter responses at each scale. An arbitrary filter response g_n with its equivalent representations is shown, and its phase deviation is labeled.

Figure 2 illustrates the phase deviation $_n$ of an arbitrary response vector g_n. The phase deviation weighting function is based the angular distance between the phase angles and is formulated as

$$_n = \frac{1}{2}(\cos(_n) \; j \sin(_n)j + 1) \qquad (9)$$

and plotted in Fig. 7,

As the magnitude and phase deviation is to be calculated at each point and at each scale in the image, the calculation is simplified to remove trigonometric equations and

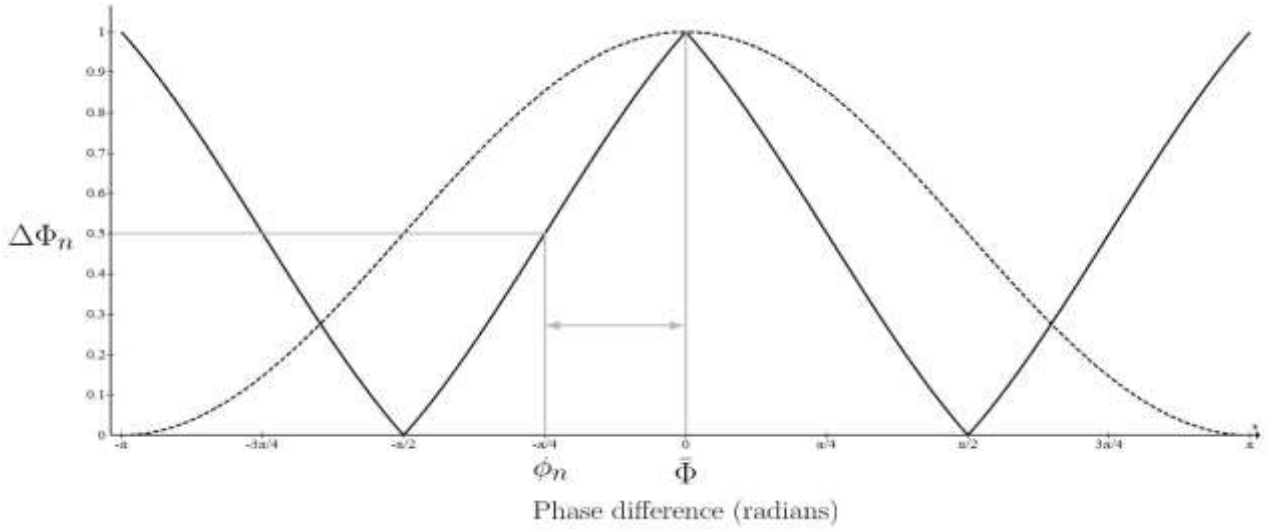

Figure-3: A comparison of the cosine distance function (dashed line) and the phase deviation measure (solid line). The phase deviation weighting $_n$ is calculated using the difference of the phase responsen and the mean phase angle over all scales.

Costly divisions. The expansion and modified function are stated as

ISSN:0971-1260

Vol-22-Issue-22-December-2019

$$A_{n\ n} = \overline{e_n + o_n} \quad \cos(\ _n) \ j \sin(\ _n)j \qquad (10a)$$

$$A = e_n e + o_n o \quad o_n e \quad e_n o : \qquad (10b)$$

Each filter response contributes $A_{n\ n}$ | magnitude, weighted by its consensus with the mean phase angle | to the phase congruency measure. However, as natural image contain noise, the response of each filter needs to be significant enough to be distinguishable from noise.

Compensating for noise in the signal

Normalisation is required in any adaptive measure, although this induces a sensitivity to noise . Image noise is assumed to be additive and features (edges and corners) are assumed to be sparse and isolated so that they may be distinguished from background noise. In order to quantify the expected noise level within the image, the response magnitude of the filter with the smallest spatial extent (making it the most sensitive to noise) is used to establish a noise floor.

The magnitude of the noise follows a Rayleigh distribution . The noise threshold

T can be tuned in terms of standard deviations from the mean of this distribution.

Calculating phase congruency

The phase congruency measure P C is calculated at each point x in the signal as

$$P\,C(x) = \frac{W(x)\ nbA_n(x) \quad _n(x)\ T\ c}{nA_n(x) +} \qquad :(11)$$

At each scale n, the filter response magnitude A_n is weighted for phase deviation $_n$ and reduced by the estimated noise floor T . A thresholding operation $bA_n(x)\ _n(x)$

T c is applied at each scale of filter response. The b c notation indicates that if the enclosed result is negative (the filter response lying below the noise floor) then the result is equal to 0 else it is left unchanged. The summation in the numerator then is normalised using the filter response magnitudes in the denominator (is a very small constant to avoid division by zero). The entire calculation is then weighted for frequency spread W (x).

The result of the phase congruency measure, is a value between 0 and 1 that indicates the significance of the underlying structure (degree of congruency) of a one dimensional signal.

Congruency over multiple orientations

Extending the phase congruency theory into two dimensions requires a modification of the log-Gabor filter bank to include orientation selectivity. The aim is to apply the one dimensional theory in discrete orientations and then combine the oriented results into a descriptive quantity for each pixel.

Directional filter bank design

Two dimensional (spatial) Gabor filters are used to extract local frequency content (band-pass) in discrete directions . Gabor filters are extended to two dimensions

as follows:

$$g_e(x) = \frac{1}{2\ x\ y} e^{\frac{1}{2}\left(\frac{x^2}{x} + \frac{y^2}{y}\right)} \cos(2\ !_{x0}\ x + 2\ !_{y0}\ y) \qquad (12a)$$

ISSN:0971-1260

Vol-22-Issue-22-December-2019

$$g_o(x) = \frac{1}{2\,\sigma_x\,\sigma_y} e^{-\frac{1}{2}\left(\frac{x^2}{\sigma_x^2}+\frac{y^2}{\sigma_y^2}\right)} \sin(2\pi f_{0x} x + 2\pi f_{0y} y): \qquad (12b)$$

Figure 4 shows a contour plot of the spatial log-Gabor filter over multiple scales; it can be seen that log-Gabor filters have a logarithmic Gaussian pro le in the radial direction (outwards from center) and a standard Gaussian pro le in the angular direction.

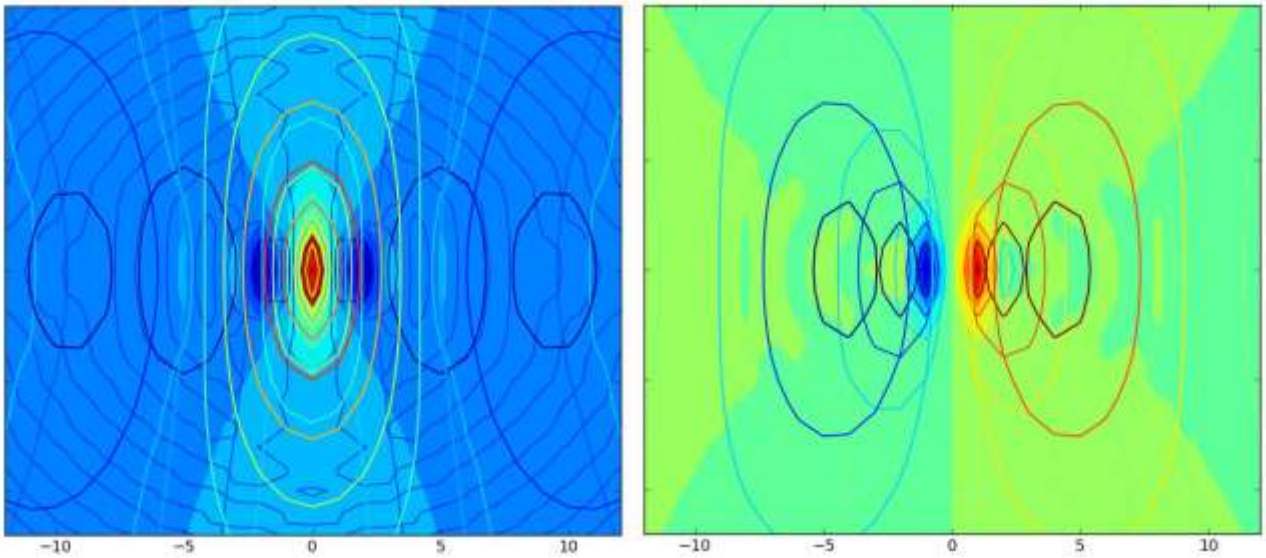

Figure-4: A false-colour contour plot showing the superimposed spatial filter responses at four scales (key: dark red is large and positive, dark blue is large and negative, unit is pixels).

By default, six discrete orientations are used which evenly divides the 0 to range as shown in Fig.5 The number of oriented filters determines the orientation selectivity; however, increasing the number of orientations significantly increases computation time with little added value . Figure 10shows the log-Gabor frequency response contours for 6 orientations at 4 scales.

Fifilter bank design is a trade-o between uniform and efficient coverage of the spectrum. In order to obtain uniform coverage, every point of the range of frequencies we want to capture must be uniformly weighted when the filter responses are summed; this requires frequency-adjacent filters to overlap (as illustrated in Fig.6. However, this overlap reduces the efficiency of our encoding as the filters become less independent and more correlated . The extension to two dimensions necessitates the inclusion of sigma parameters to control radial and angular spread. The parameters suggested by Kovesi are provided.

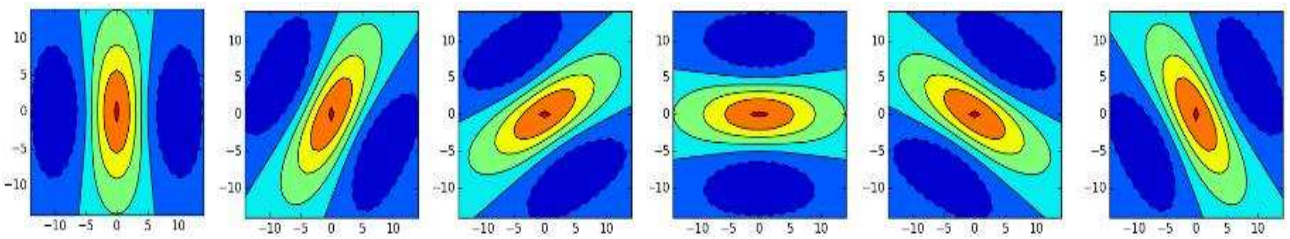

(a) Even oriented filter set.

ISSN:0971-1260

Vol-22-Issue-22-December-2019

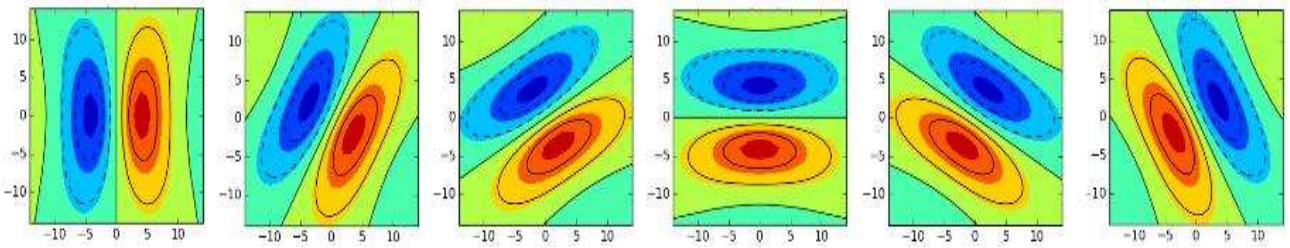

(b) Odd oriented filter set.

Figure-5: Even and odd spatial filter responses at six orientations at a single scale (key: dark red is large and positive, dark blue is large and negative, unit is pixels).

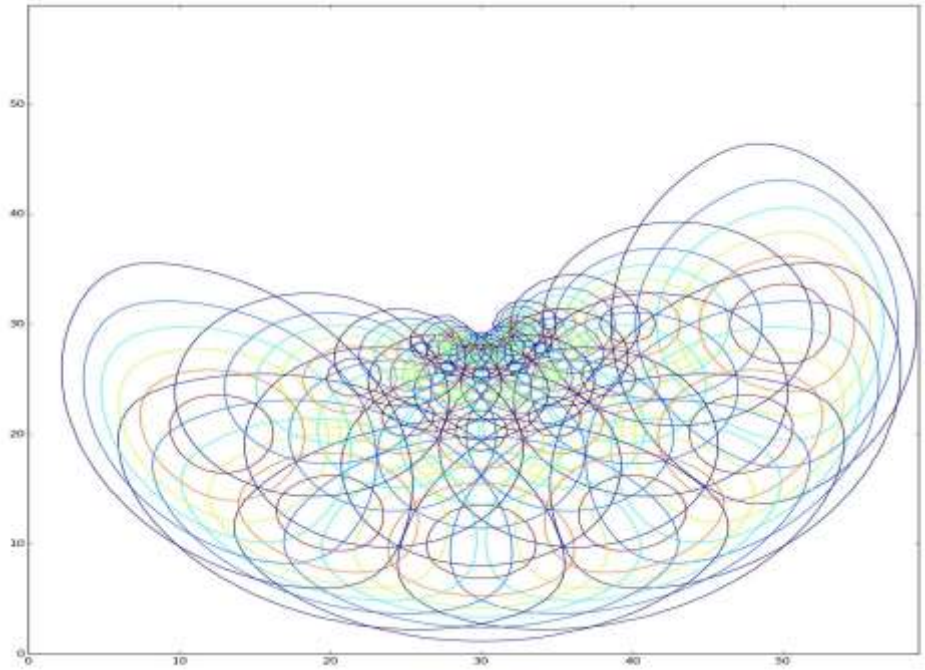

Figure-6: A contour plot showing one-sided superimposed oriented spatial frequency responses of the log-Gabor filter bank in the Fourier domain. Note the angular and radial overlap that forms a part of the design trade-o s towards uniform spectrum coverage.

As an alternative to the discrete directional filters used in Kovesi's phase congruency, Mellor , use steerable band-pass filtering (a difference of Gaussians operation followed by the Hilbert transform) to recover the symmetric phase information. The non-linear log-Gabor filters used in Kovesi's phase congruency are not steerable, which is why calculation in discrete orientations is required.

Oriented phase congruency

Phase congruency is calculated at each orientation using

$$P\,C(x)_i = \frac{{}_nW\,(x)\,bA_n(x)\quad {}_n(x)\;\;T\;c}{{}_nA_n(x)\;+} \qquad (13)$$

This equation is essentially unmodified from the one dimensional analysis, although oriented components have been appended with a subscript i to indicate that the calculation is specific to each orientation. Note that the noise floor T and the mean phase angle quantities are calculated for each orientation. For the remainder of this report, oriented components are subscripted with i; most notably, the phase congruency P C_i and the mean phase angle $_i$ quantities are collectively referred to as the oriented components of phase congruency.

ISSN:0971-1260

Vol-22-Issue-22-December-2019

Figure 7 demonstrates the relationship between the phase (i.e. the ratio of the quadrature filter responses) and the underlying structure. The four images show different phase responses of a = =2 oriented filter which have been created using

P (x; y) = $e_{n;i}$(x; y) + $o_{n;i}$(x; y) (14)

where each pixel in the image P is a sum of the spatial filters weighted with + = 1. In the phase congruency equation, the mean phase angle represents the consensus of the structure recovered by a particular oriented filter over all scales.

Another reason for the inclusion of Fig. 7 is to emphasise the important distinction between the angle representing the mean phase response $_i$, and the filter orientation $_i$. The magnitude of congruency P C_i is associated with the direction of the filter,

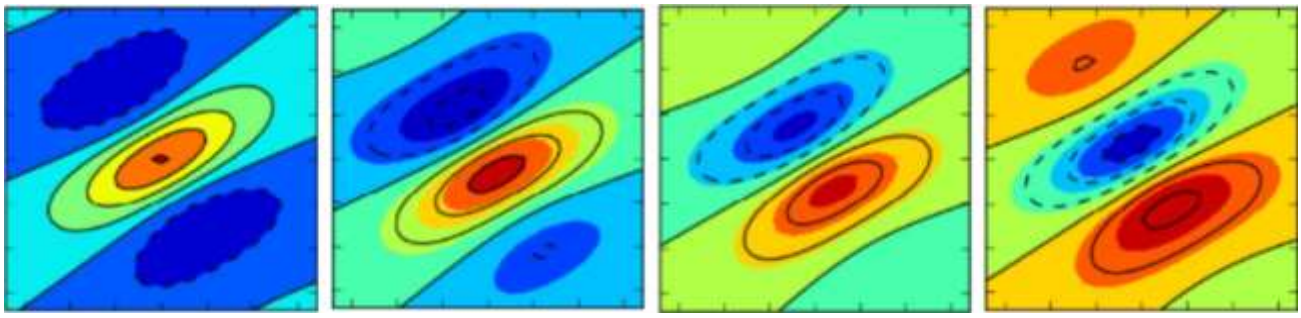

(a)= 0.(b) = =2.(c)=(d)= 3 =2.

Figure-7: A sequence of contour plots of the spatial log-Gabor filter response, illustrating the relationship between phase and structure; each representation of the oriented (= =2) filter is constructed using a different ratio of the quadrature pair. (Key: dark red is large and positive, dark blue is large and negative, unit is pixels.) and is represented as a vector at angle $_i$. Visualising the oriented components in this way is useful in the next section, which presents a method for combining the values to describe structural features in images.

Representation using a reduced feature set

The components a, b and c represent summations of the phase congruency magnitudes

P C_i calculated with Eq.(11) at each orientation $_i$, and are calculated as

a = $_i$(P C_i cos($_i$))^2 (16a)

b = 2 $_i$(P C_i cos($_i$))(P C_i sin($_i$)) (16b)

c = $_i$(P C_i sin($_i$))^2: (16c)

The maximum moment indicates feature (i.e. edge) significance and is used to create an edge map of the image . If both moment values are large, the point is classified as a corner; consequently, the corner features present in the image are a subset of the edge map. The angle of the principal axis indicates the orientation of the edge and is calculated as follows:

^{0} = $_2$atan a c : (4.17)

1 b

Together, the three components of the reduced feature set at each pixel describe the structural make-up of a scene. These components are an integral part of the methods developed in the remaining chapters of this work.

ISSN:0971-1260

Vol-22-Issue-22-December-2019

Figure 8 has been included to show how the oriented congruency components, P C_i, are described by the reduced feature set. On the right of Fig. 8 the maximum moment with scalar magnitude M and direction ^{0} values can be seen to describe the significance and orientation of the curved edge; the minimum moment, m, describes the `cornerness' due to the curve in the edge. Of the six orientations used in analysis, only three were non-zero. The non-zero P C_i magnitudes are shown as vectors on the curved edge (i.e. P C_1, P C_2 and P C_3), and the phase response of each is represented as contour plots on the left (i.e. $_1$, $_2$ and $_3$).

The remaining sections of this report present an analysis of phase congruency as a tool for exposing invariant structure and predictable features in multi-spectral images.

Identifying predictable image elements

The primary objective of the investigation carried out in this paper is to extract repeatable and predictable structural elements using the phase congruency process. Supervised learning is used to identify predictable relationships between components extracted from corresponding observations in the two spectra.

This provides a brief overview of the support vector machine model for supervised learning. Methods to characterise the performance of the learning model are then introduced to quantify predictability of image elements describes the approach undertaken to investigate predictability in multi-

spectral information, and the tools and parameters used in the investigation are recorded .

Support vector machines

Support Vector Machine (SVM) are a class of supervised learning models used in a broad array of applications. They are regarded as one of the best o -the-shelf algorithms for supervised learning and are widely used in multi-spectral and remote-sensing literature [52, 75]. A strong motivation for the use of SVM algorithms in this context is the high accuracy that is achieved with a limited amount of training data [76].

Supervised learning is an iterative process. Sample data with known classes (or labels) is used to train the SVM model which is a hyperplane that separates the classes. This hyperplane is called the decision boundary, and is used to classify future (unlabelled) samples. Due to the strict requirement of linear separability of classes, a kernel mapping is commonly applied to accommodate data that requires a more complex decision boundary [52]. Figure 13 shows a visualisation of three different SVM kernels applied to the same training data on a two dimensional plane. Each training sample is shown as a circle on the plane with a colour indicating its class (black or white). These samples are used to generate a decision boundary, shown as a solid black line, separating the two classes; the shaded levels of grey indicate the confidence with which the SVM classifies each coordinate in the plane (from black to white).

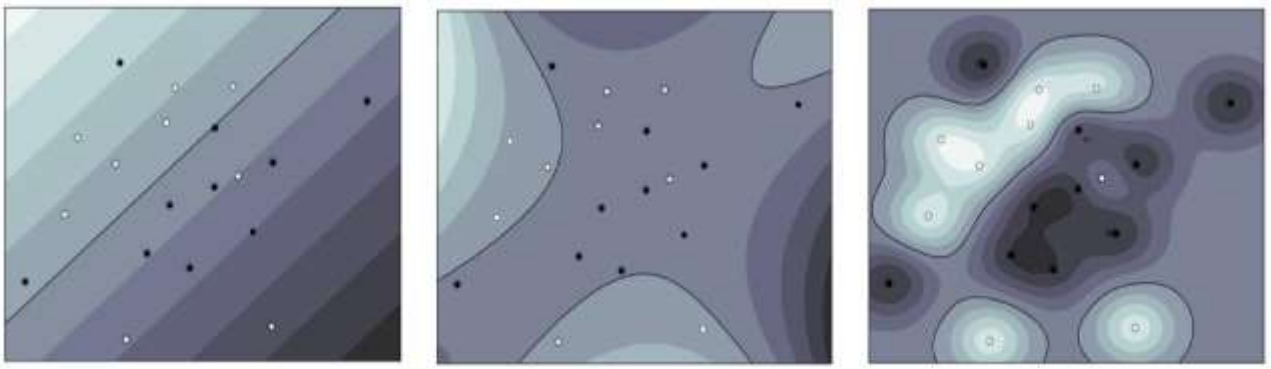

(a) Linear kernel. (b) Polynomial kernel. (c) Radial Basis Function (RBF) kernel.

Figure 9: Three SVM kernel variations used to extend the functionality of linear SVM Classification to non-linearly-separable data distributions. The three SVM kernels shown in Fig. 9 generate different decision boundaries, which represent different hypotheses that an arbitrary point on the plane will belong to a certain class. In this way, SVMs can be used to discover predictable behaviour and relationships in high dimensional data by formulating and testing different hypotheses.

Characterizing performance

ISSN:0971-1260

Vol-22-Issue-22-December-2019

The approach to achieving the objectives of this chapter is to use supervised learning with SVMs to identify predictable structure in visible and thermal images; this section describes how the hypotheses are evaluated and what the results can tell us. Three different SVM kernels are used to discover simple (linearly separable) to complex (polynomial and RBF kernels) relationships between components of the phase congruency process.

The trained SVM is required to classify whether two points taken from the different spectral modalities correspond to the same observation in the scene. This is a Classification problem to determine if a single pattern vector (a string of numbers composed of values taken from the two points) is indicative of a match or not. To accomplish this, the model requires a set of positive and negative training examples to establish the decision boundary. A training example is a pattern vector with a known class based on the known relationship between the points (i.e. whether the two points used to construct the pattern vector are corresponding observations of the same point or not).

The process of evaluating the hypothesis proposed by the SVM kernel is called testing. A portion of positive and negative samples are kept aside during the training process for use in hypothesis testing. SVM performance is characterised by comparing the Classification assigned by the hypothesis to the known class of each sample. Samples with correctly-assigned labels are referred to as true positives and true negatives, while errors in Classification are referred to as false positives (incorrectly matched) and false negatives (incorrectly rejected).

Associated with each Classification is a numerical value indicating the probability of class membership. By continuously varying a threshold on this probability, a Receiver Operating Characteristic (ROC) plot can be constructed to characterise the effectiveness of the SVM hypothesis. The number of True positive (TP), True negative (TN), False positive (FP) and False negative (FN) element counts are combined to form the True positive rate (TPR)

RESULTS

The objectives stated at the beginning of this chapter were two-fold: to establish an invariant representation of repeatable features of visible and thermal information, and to identify predictable relationships between values extracted in the phase congruency analysis process. The results of these two investigations are presented in this section; A representation of the maximum and minimum moment values, which provide an edge and a corner map respectively, are shown in Fig. 16 The purpose of achieving an invariant representation is to enable methods that describe and match visible similarity to be used with multi-spectral information; therefore, the effectiveness of this representation can only be analysed in terms the performance it grants to these methods. The results presented here are the basis for the development work carried out and the evaluation of the invariant representation provided by phase congruency is deferred to its application.

Predictable components of congruency

STRUCTURE OF THE INVESTIGATION

The aim of this investigation is to identify a pattern vector that has a predictable relationship across the spectral modalities. Figure provides a ow diagram of how the results are organised. The notation for each component is appended with an image identifier (i.e. 1 or 2) and directional filter orientation indexed by i (e.g. 1_0 represents the mean phase calculated with the directional filter-bank at orientation i = 0 from image 1). The components are initially partitioned into the oriented and reduced feature sets and analysed separately in blocks I and II; predictable components in each of these sets are identified and then combined in block III. Dashed lines indicate that the elements of the pattern vector were modi ed in some way (e.g. multiplied), and solid lines indicate that the pattern vectors were concatenated. Each transition is motivated by the performance, which is demonstrated with the ROC curve, offered by the new pattern vector.

(a) Original thermal image. **(b) Original visible image.**

ISSN:0971-1260

Vol-22-Issue-22-December-2019

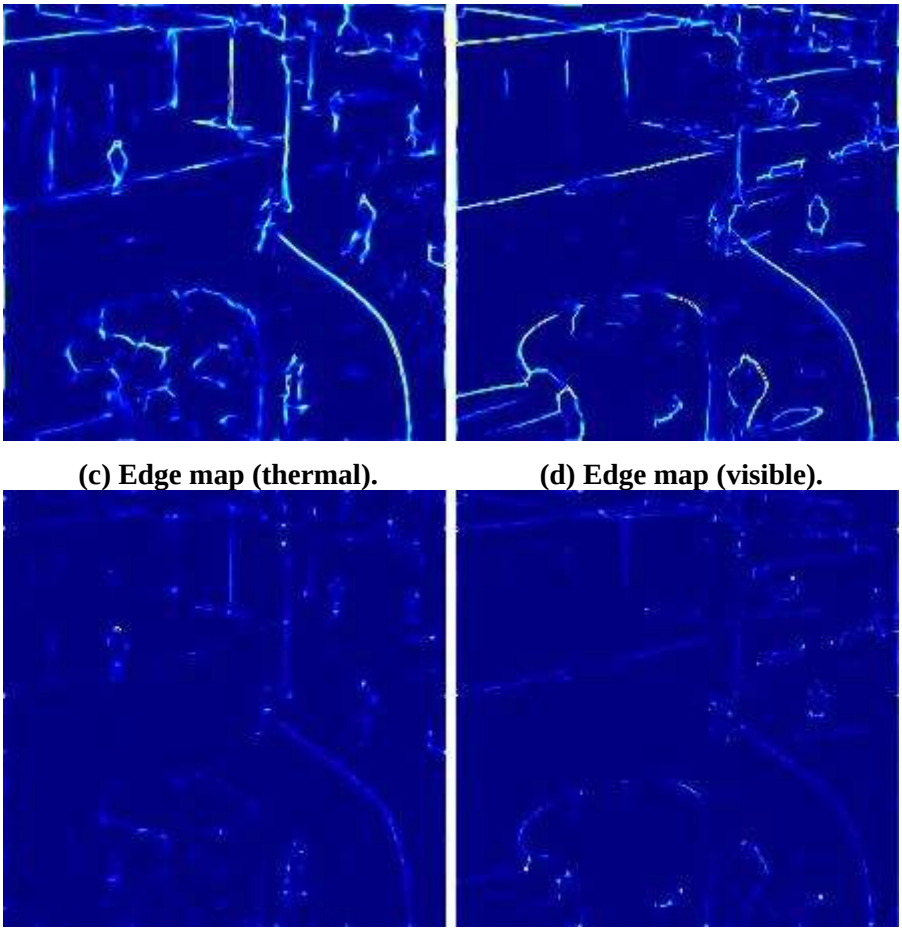

(c) Edge map (thermal). **(d) Edge map (visible).**

Figure-12: The edge and corner maps of the reduced congruency feature set form the invariant representation of this project. (Modified images from the OSU database [44].)

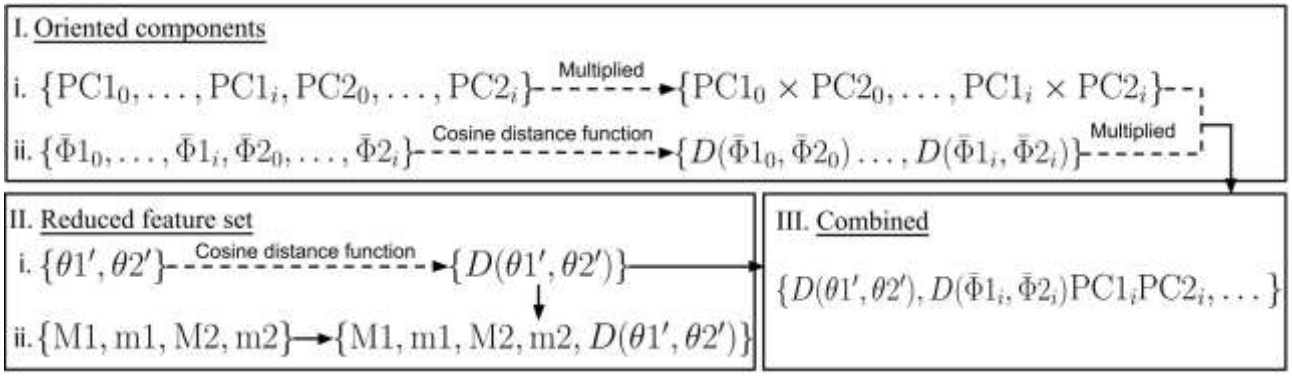

Oriented components

The oriented components of phase congruency, refer to the separate outputs of the six directional filter banks. The phase congruency and mean phase angles, introduced in Eq. (13) and Eq. (8) respectively, are used to form pattern vectors in the following experiments.

Figure shows the ROC plots for the pattern vectors of the separate congruency and mean phase angles. The performance of both pattern vectors indicate no predictive value beyond random guessing (the ROC plots are along the diagonal).

(a) Oriented congruency magnitudes PC_i. **(b) Oriented mean phase angles $_i$.**

ISSN:0971-1260

Vol-22-Issue-22-December-2019

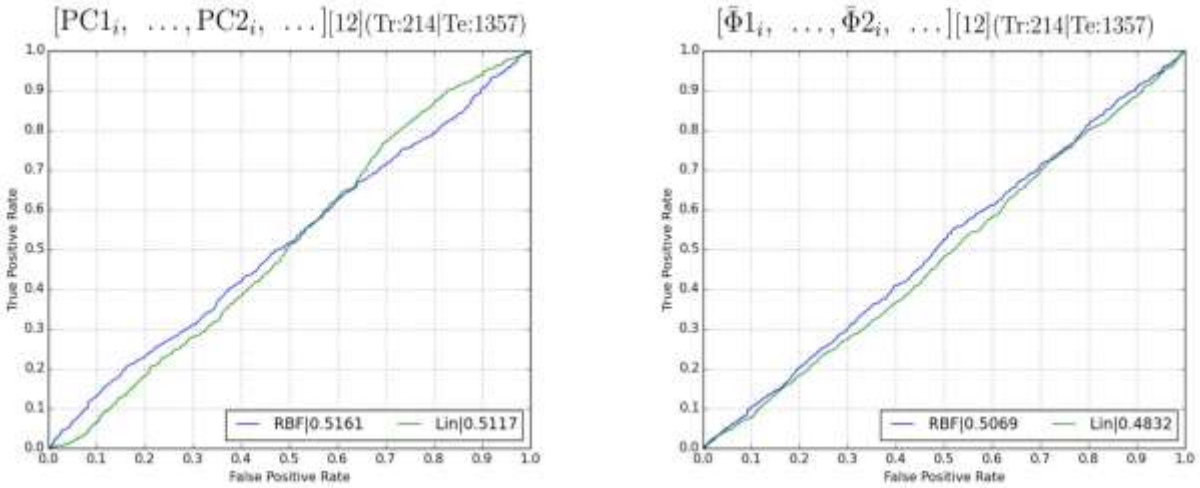

Figure-9: ROC plots of the twelve separate oriented components of the phase congruency magnitudes and mean phase angles (i.e. concatenation of outputs of six orientations from two images).

The result shown in Fig.9 is used to demonstrate the performance offered by combining elements, shown as dashed lines in Fig. reported in Fig. 11 The magnitude of oriented congruency P C_i provides an indication of structural significance (i.e. above the noise circle and consensus over multiple scales); for this reason, the congruency at corresponding orientations is combined by multiplication to ensure that the resulting product is non-zero if the oriented congruency from both modalities is non-zero. The results are reported in Fig. 19 and show an appreciable improvement on the separate components of Fig. 18 The angular mean phase components are combined using the cosine distance measure; however, only a small improvement over Fig. 18 can be seen in their combination in Fig. 19.

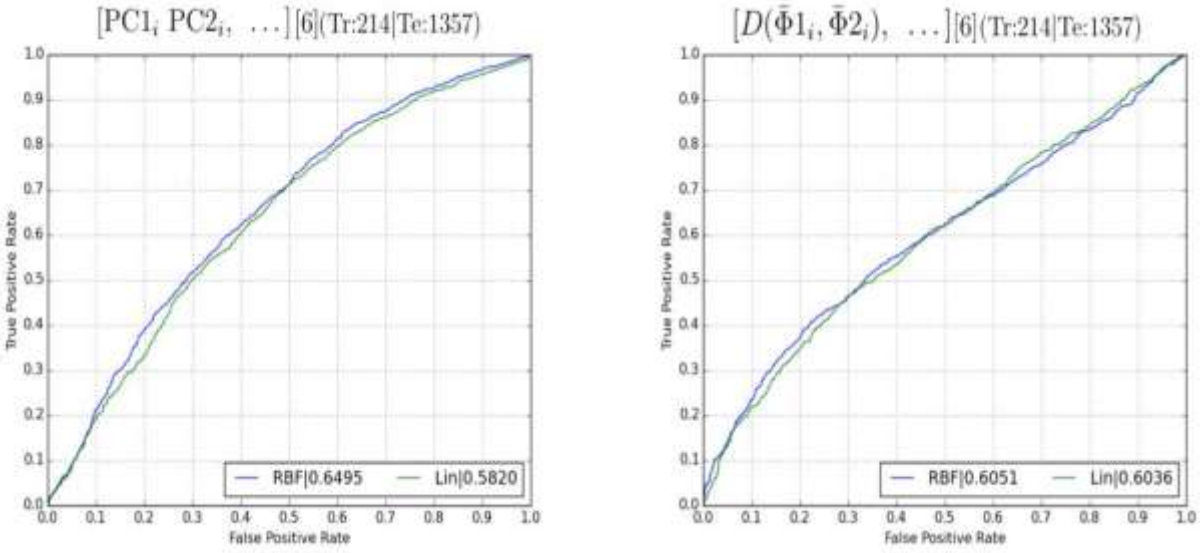

Figure-10: ROC plots demonstrating the performance of corresponding oriented components, extracted from each spectral modality, combined using multiplication (in the case of congruency) or cosine distance (in the case of phase).

The two results presented in Fig. 10 are combined by multiplying each respective oriented component; therefore, each component of the resulting vector is only large if the structures are similar (angular phase distance) and significant in both modalities. An improvement in prediction with the linear kernel using this combined pattern vector is shown in Fig. 10

Reduced feature set

ISSN:0971-1260

Vol-22-Issue-22-December-2019

The second group of components investigated is the reduced feature set which was introduced the ROC curves of the moment magnitudes and feature orientation pattern vectors are shown in Fig. 10 Figure that the feature orientation components are not linearly separable, but are separable with the RBF kernel. In order to make the components linearly separable, the cosine distance function is applied; the resulting ROC curve is shown in Fig 11

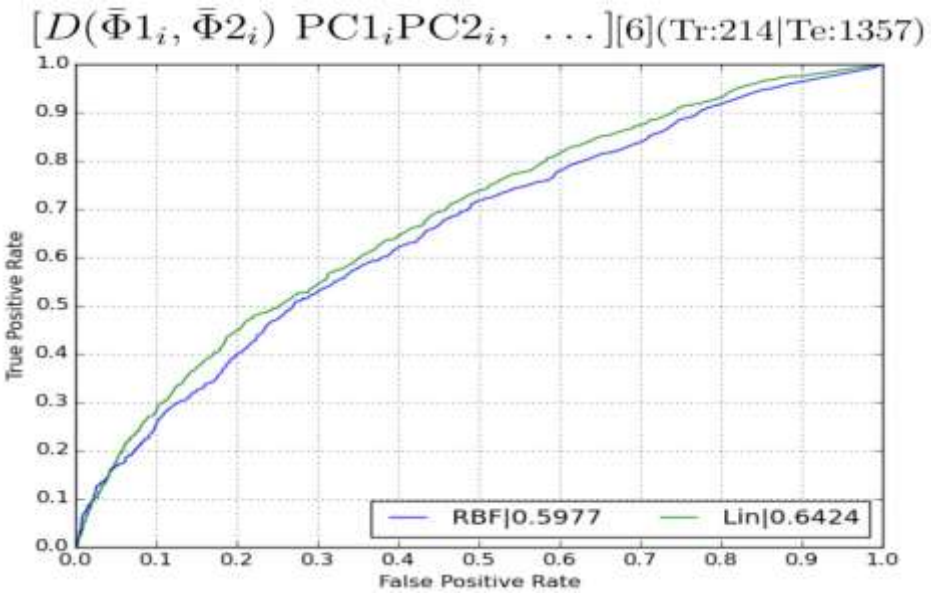

Figure-10: The oriented congruency and phase components are multiplied to form a single pattern vector. Each of the six (oriented) elements of the pattern vector represents the similarity of structure (phase angle) and weighted by the significance of the structure in both images (congruency magnitude

(a) Maximum and minimum moment (b) The angle of the maximum moment ^{0}. magnitudes.

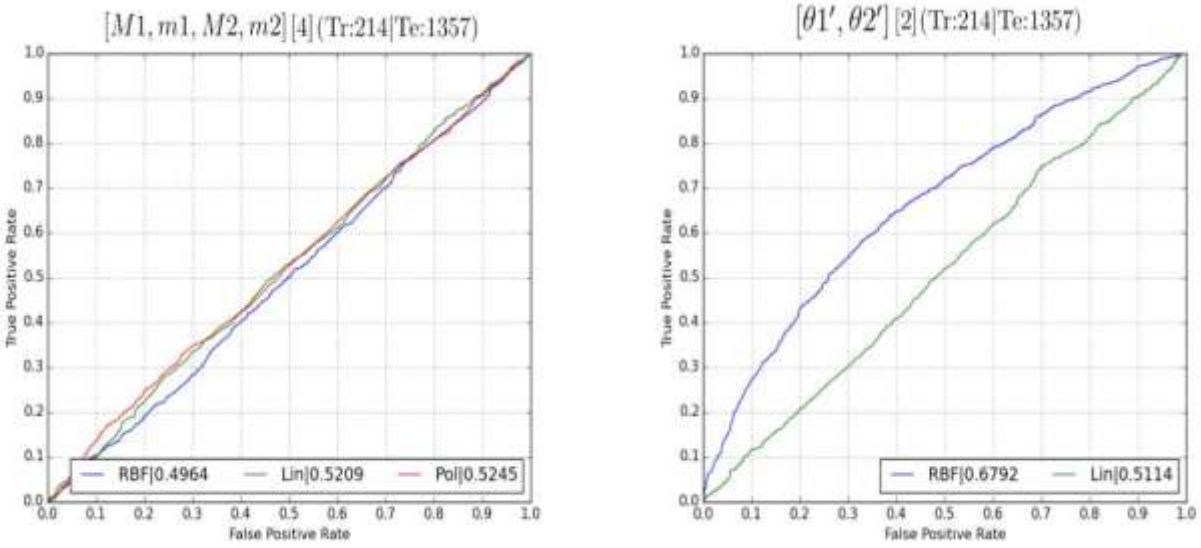

Figure-11: Two ROC plots analysing the separate elements of the reduced feature set. Plot

(a) shows the performance of the maximum and minimum moment magnitudes, which indicate the presence of a feature. The pattern vector analysed in

(b) consists of the edge orientations (Angle of the principal axis) from each image.

REFERENCES

ISSN:0971-1260

Vol-22-Issue-22-December-2019

[1] D. Ziou, C. Armenakis, and D. Li, \A comparative analysis of image fusion meth-ods," IEEE Transactions on Geoscience and Remote Sensing, vol. 43, pp. 1391{ 1402, June 2005.

[2] J. B. Campo, \Multimodal Stereo from Thermal Infrared and Visible Spectrum," PhD thesis, Universitat Autonoma de Barcelona, Spain, 2012

[3] M. Govender, K. Chetty, and H. Bulcock, \A review of hyperspectral remote sensing and its application in vegetation and water resource studies," Water SA, vol. 33, no. 2, 2009.

[4] M. Moganti, F. Ercal, C. H. Dagli, and S. Tsunekawa, \Automatic PCB In-spection Algorithms: A Survey," Computer Vision and Image Undefirstanding, vol. 63, pp. 287{313, Mar. 1996.

[5] H. Loh and M. Lu, \Printed circuit board inspection using image analysis," IEEE Transactions on Industry Applications, vol. 35, no. 2, pp. 426{432, 1999.

[6] A. Wong and W. Bishop, \E cient least squares fusion of MRI and CT images using a phase congruency model," Pattern Recognition Letters, vol. 29, pp. 173{ 180, Feb. 2008.

[7] F. Maes, A. Collignon, D. Vandermeulen, G. Marchal, and P. Suetens, \Mul-timodality image registration by maximization of mutual information," IEEE transactions on medical imaging, vol. 16, pp. 187{98, Apr. 1997.

[8] J. P. W. Pluim, A. Maintz, and M. A. Viergever, \Mutual-information-based reg-istration of medical images: A survey," IEEE Transactions on Medical Imaging, vol. 22, no. 8, pp. 986{1004, 2003.

[9] Z. Liu, D. S. Forsyth, and R. Laganiere, \A feature-based metric for the quanti-tative evaluation of pixel-level image fusion," Computer Vision and Image Understanding, vol. 109, pp. 56{68, Jan. 2008.

[10] C. Pohl and J. L. Van Genderen, \Multisensor image fusion in remote sensing: Concepts, methods and applications," International Journal of Remote Sensing, vol. 19, no. 5, pp. 823{854, 1998.

[11] A. Rogalski, \History of infrared detectors," Opto-Electronics Review, vol. 20, no. 3, pp. 279{308, 2012.

[12] M. Iqbal, An introduction to solar radiation. Elsevier, 1983.

[13] P. Ricaurte, C. Chilan, C. A. Aguilera-Carrasco, B. X. Vintimilla, and A. D. Sappa, \Feature point descriptors: Infrared and Visible Spectra," Sensors 2014 (Switzerland), vol. 14, pp. 3690{3701, 2014.

[14] R. Fattal, \Single image dehazing," ACM Transactions on Graphics, vol. 27, no. 3, p. 1, 2008.